Numerical Simulation of Breaking Waves by Large Eddy Simulation and VOF Method

Qun Zhao[1] and Katsutoshi Tanimoto[2]

Abstract

In this paper, the VOF method for free surface flow is applied to simulate breaking waves incident on a submerged reef. An efficient numerical wave channel with two absorbing boundaries is developed. Corresponding boundary conditions are prescribed. Smagorinsky's sub-grid scale model is incorporated to account for the sub-grid scale turbulence. Numerical results are compared with laboratory measurements.

Introduction

Owing to the extremely complicated wave manner caused by the wave non-linearity and breaking, a complete satisfactory theory for wave deformation on uneven topographies seems to be not attainable so far. Small-scale model tests and field observations are still dominant in the traditional study. Nevertheless, small-scale model tests suffer from the scale effects, while large-scale model tests are too expensive.

The booming progress in computer technology in the past decade witnesses the continuous improvements in computational fluid dynamics. With today's personal computer, it is possible to solve the Naiver-Stokes equations for coastal engineering problems.

The VOF method developed by Hirt and Nichols(1981) is among the best candidates for solving free surface flow problems due to its clearness and simplicity of

---
[1]Post doctoral fellow, Dept. of Civil Eng., Saitama Univ., Shimo-Okubo 255, Urawa, Saitama 338-8570, Japan. E-mail:zhao@envi.env.civil.saitama-u.ac.jp
[2]Professor, ditto. Tel/Fax:+81-48-858-3561, E-mail:tanimoto@envi.env.civil.saitama-u.ac.jp

tracing free surface. Besides, this method is especially useful for calculating break-ing waves, since the free surface is not necessarily required to be single. Several studies based on the VOF method to simulate breaking waves have been reported recently(van der Meer et $al.$, 1992; Lemos, 1992; Petit et $al.$, 1994; van Gent et $al.$, 1994; Sabeur et $al.$, 1996; Kawasaki and Iwata, 1997; Lin and Liu,1998; etc.).

However, most of these studies either ignore the sub-grid scale turbulence to-tally, which implies that the sub-grid scale energy dissipation purely relies on the numerical viscosity appeared in the finite difference schemes; or use a con-stant eddy viscosity of the same order as that of Reynolds Averaged Navier-Stokes(RANS) equations.

Lemos(1992), Lin and Liu(1998) demonstrate two-dimensional breaking wave models based on the Reynolds Averaged Navier-Stokes equations separately. Both of them used the $k - \varepsilon$ model with standard coefficients. Lemos used a linear clo-sure for the Reynolds stress terms, while Lin and Liu used a nonlinear closure to account for the anisotropic turbulence. Nevertheless, Lemos' results were not compared with experimental measurements directly. Lin and Liu's results showed that their model could give generally good agreement at the inner surf zone. Near the breaking point, however, the $k - \varepsilon$ model always overestimates the eddy vis-cosity, and thus leads to an underestimation of surface elevation. If we consider the breaking point is the transition point from laminar flow to turbulent flow, this in one way suggests the limitation of the $k - \varepsilon$ model in predicting the flow transition. Besides, there are too many coefficients in the $k - \varepsilon$ model, and this makes it difficult for calibration.

In the present paper, therefore, we are trying to use a space filter to account for the sub-grid scale turbulence. It is expected that the sub-grid scale turbulence is more isotropic and less flow dependent, therefore, the closure model can be simpler and less sensitive to the parameterization. However, due to the very high Reynolds number and limited computer resources, we restrict the present study to two-dimensional problem.

Numerical Formulation

The governing equations are the mass conservation equation for incompressible flows:

$$\frac{\partial u_j}{\partial x_j} = 0 \tag{1}$$

and the Navier-Stokes equations:

$$\frac{\partial u_i}{\partial t} + u_j \frac{\partial u_i}{\partial x_j} = -\frac{1}{\varrho}\frac{\partial p}{\partial x_i} + \nu\frac{\partial}{\partial x_j}[(\frac{\partial u_i}{\partial x_j} + \frac{\partial u_j}{\partial x_i})] + g_i \tag{2}$$

in which ϱ and ν are the fluid density and kinematic viscosity, respectively. g_i is the gravitational acceleration at the ith direction, u_i is the velocity component, and p is the pressure. Here $i = 1, 2$ correspond to horizontal (x) and vertical (z) directions, respectively, j is dummy.

Assuming that the sub-grid scale turbulence is isotropic, the filtered Navier-Stokes equations and the continuity equation read:

$$\frac{\partial \overline{u}_j}{\partial x_j} = 0 \tag{3}$$

$$\frac{\partial \overline{u}_i}{\partial t} + \overline{u}_j \frac{\partial \overline{u}_i}{\partial x_j} = -\frac{1}{\rho}\frac{\partial \overline{p}}{\partial x_i} + \nu \frac{\partial}{\partial x_j}[(\frac{\partial \overline{u}_i}{\partial x_j} + \frac{\partial \overline{u}_j}{\partial x_i})] - \frac{\partial}{\partial x_j}(\overline{u_i u_j} - \bar{u}_i \bar{u}_j) + g_i \tag{4}$$

The top-hat filter(cell volume) is applied in the above equations, and the over-bars denote the resolvable scale quantities (for example $\overline{u}_i$):

$$\overline{u}_i(x, z, t) = \frac{1}{\Delta x \Delta z} \int_{x-\frac{1}{2}\Delta x}^{x+\frac{1}{2}\Delta x} \int_{z-\frac{1}{2}\Delta z}^{z+\frac{1}{2}\Delta z} u_i(\zeta, \eta, t) d\zeta d\eta \tag{5}$$

Where Δx and Δz are the mesh sizes of the finite- difference equations in x and z directions, respectively. The $\overline{u}_i$ is the filtered velocity component; $\overline{p}$ is the filtered pressure. The new terms appeared in the filtered equations are:

$$(\overline{u_i u_j} - \bar{u}_i \bar{u}_j) = L_{ij} + C_{ij} + R_{ij} \tag{6}$$

with L_{ij}, C_{ij}, R_{ij} referred as the Leonard term, the cross term and the sub-grid scale(SGS) Reynolds term, respectively:

$$L_{ij} = \overline{\bar{u}_i \bar{u}_j} - \bar{u}_i \bar{u}_j \tag{7}$$

$$C_{ij} = \overline{\bar{u}_i u'_j} + \overline{u'_i \bar{u}_j} \tag{8}$$

$$R_{ij} = \overline{u'_i u'_j} \tag{9}$$

The prime denotes a SGS quantity. Notice that the sum of the Leonard term and the cross term $(L_{ij} + C_{ij})$ is small comparing with the SGS Reynolds stress (Deardorff, 1970), and thus can be neglected. Therefore, we finally obtain the filtered Navier-Stokes equations in which the SGS Reynolds stress need to be modeled.

Applying Boussinesq's eddy-viscosity hypothesis, the SGS Reynolds stress is given by:

$$R_{ij} = -2\nu_T S_{ij} \tag{10}$$

where

$$S_{ij} = \frac{1}{2}(\frac{\partial \overline{u}_i}{\partial x_j} + \frac{\partial \overline{u}_j}{\partial x_i}) \tag{11}$$

is the strain rate tensor of the resolved scales. Smagorinsky's model gives:

$$\nu_T = (C_S \Delta)^2 |S| \tag{12}$$

$$\Delta = (\Delta x \Delta z)^{\frac{1}{2}} \tag{13}$$

in which ν_T is SGS eddy viscosity, Δ is SGS length scale for two-dimensional problems, and $C_s = 0.10$.

Equation (12) is used otherwise of the fluid except at the solid boundary, where the van Driest damping function is applied to the SGS length scale. At free surface, the closure for the SGS Reynolds stress is less certain, we apply Smagorinsky's model at the present stage.

Besides the above equations, a volume of fluid function (F) is used to define the fluid region in the VOF method. A unit value of F corresponds to a cell full of fluid, while a zero value indicates that cell contains no fluid. Cells with F values between zero and one represent the water-air interface. The governing equation of F function is given by:

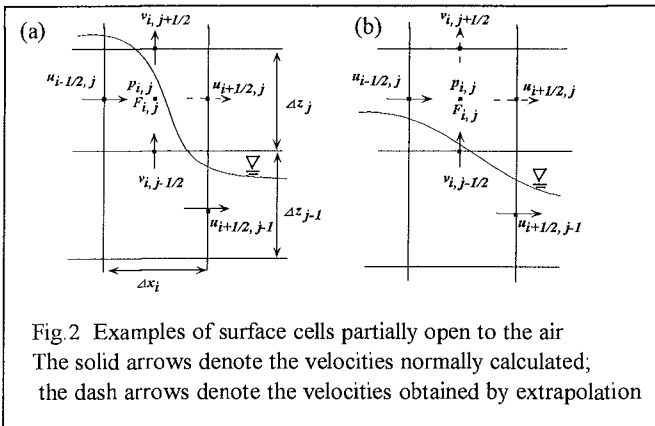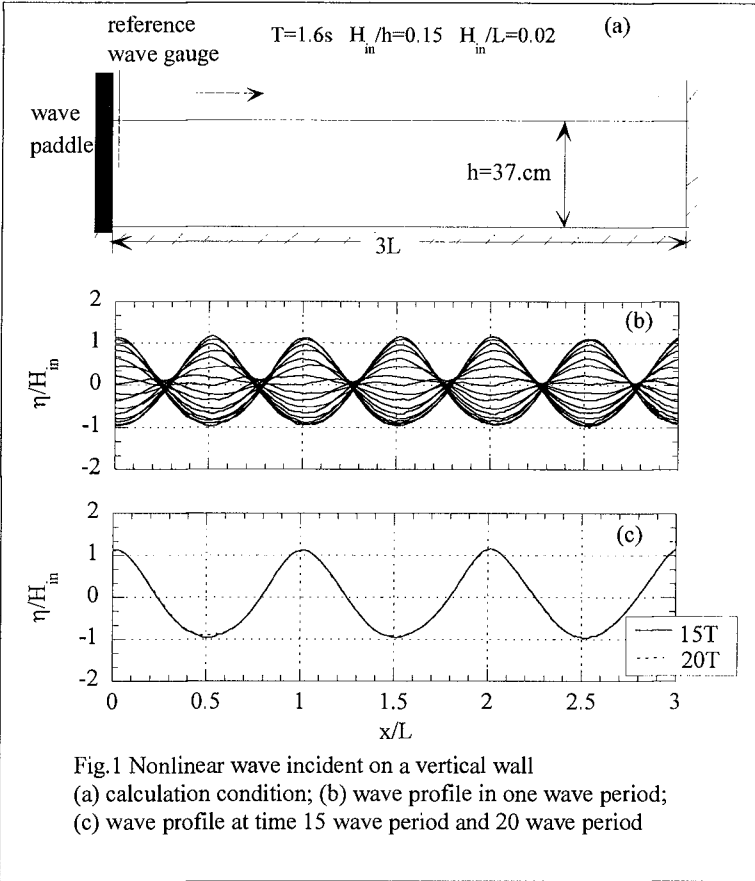$$\frac{\partial F}{\partial t} + \bar{u}_j \frac{\partial F}{\partial x_j} = 0 \tag{14}$$

Numerical Methods

The governing equations are discretized using a staggered grid where the velocities are located at the cell faces, the pressures and the F functions are settled at each cell center. The time increment is achieved by the Euler scheme and the convective terms are approximated by the third-order difference scheme due to stability consideration.

In order to obtain accurate result, boundary conditions must be treated very carefully. In the present study, the boundary conditions for resolved field have been summarized into three kinds, namely, the lateral boundary conditions, the free surface boundary conditions and the solid boundary conditions.

The lateral boundary conditions include the inflow boundary and the out flow boundary(open boundary). At the inflow boundary, we choose to generate the incident wave by simulating a piston-type wave-maker. The wave paddle is driven by the second order Stokes wave theory (Hughes, 1993), and an absorbing wave-maker system(Zhao, 1998) which is essentially same as that in the physical experiment. This method is particularly effective for our case, where waves are generated at deeper water region and encounter a reflective structure(submerged reef with a steep reef face). The secondary wave for this case is very small according to our study. The example of second order Stokes waves incident on a vertical wall is shown in Fig. 1, where T is the wave period, h is the still water depth, H_{in} denotes the incident wave height, L is the incident wavelength calculated by linear wave theory, and η is the water surface relative to the still water level.

At the open boundary, an artificial boundary condition has to be given to truncate the computational domain from the infinite physical domain, but without rendering disturbances to the inside area. For wave problems, this is normally fulfilled by the well-known Sommerfeld radiation boundary condition. However, the wave dispersion induced by wave nonlinearity and breaking makes it difficult to use one wave celerity to represent the whole wave field. Hence, a damping zone(Arai, 1993) and the Sommerfeld radiation condition are combined at the open boundary.
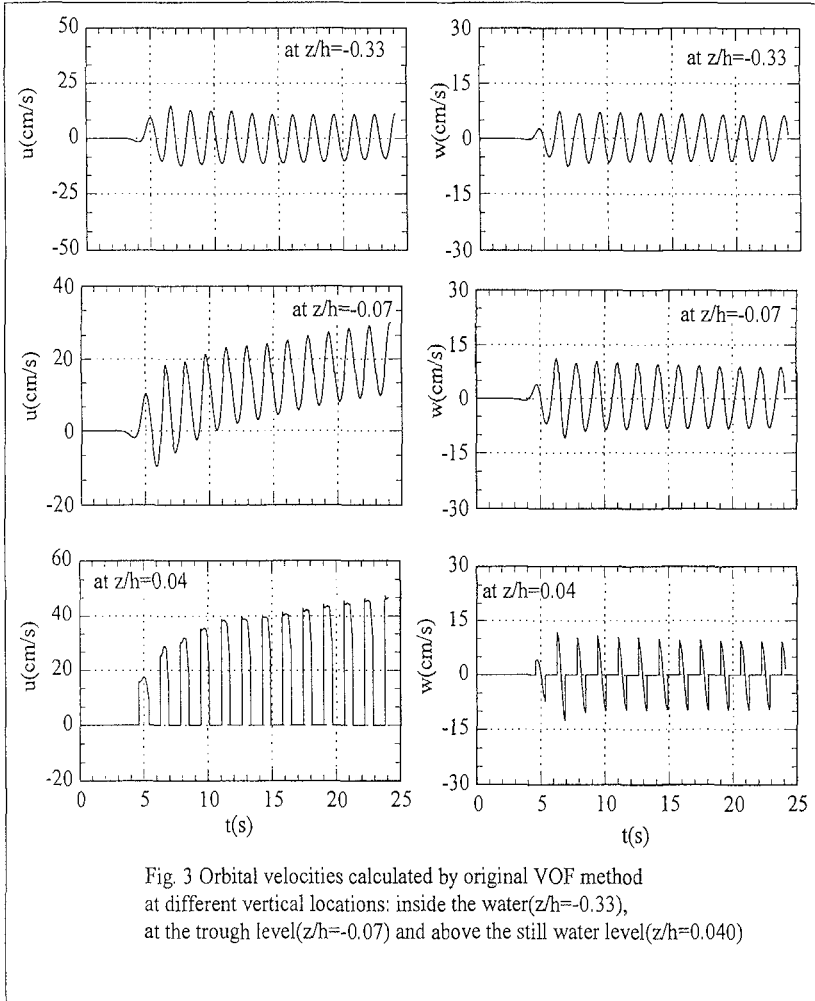
reference wave gauge   T=1.6s $H_{in}/h=0.15$ $H_{in}/L=0.02$ (a)

wave paddle

h=37.cm

3L

η/H_{in}

(b)

η/H_{in}

(c)

— 15T
··· 20T

0   0.5   1   1.5   2   2.5   3

x/L

Fig.1 Nonlinear wave incident on a vertical wall
(a) calculation condition; (b) wave profile in one wave period;
(c) wave profile at time 15 wave period and 20 wave period

(a)   (b)

$v_{i,j+1/2}$ $v_{i,j+1/2}$

$u_{i-1/2,j}$ $p_{i,j}$ $u_{i+1/2,j}$ $u_{i-1/2,j}$ $p_{i,j}$ $u_{i+1/2,j}$
              $F_{i,j}$ $F_{i,j}$

Δz_j

$v_{i,j-1/2}$ $v_{i,j-1/2}$

$u_{i+1/2,j-1}$ Δz_{j-1} $u_{i+1/2,j-1}$

Δx_i

Fig.2 Examples of surface cells partially open to the air
The solid arrows denote the velocities normally calculated;
the dash arrows denote the velocities obtained by extrapolation

Fig. 3 Orbital velocities calculated by original VOF method
at different vertical locations: inside the water(z/h=-0.33),
at the trough level(z/h=-0.07) and above the still water level(z/h=0.040)

The free surface boundary conditions include the dynamic and the kinematic boundary conditions. The dynamic boundary condition is satisfied by $\bar{p} = 0$ at the free surface. The pressures at the surface cells are calculated by linear extrapolation from the cells inside the fluid domain. The kinematic boundary condition is automatically satisfied by Eq.(14). However, special care must be paid to the treatment of velocities at surface cells . The examples are shown in Fig. 2 , where parts of the cell faces are exposed to the air. For these cases, the momentum equations for water can not be used. The determination of these values is quite arbitrary. In the original VOF method(Hirt and Nichols, 1981) and some other methods related to the VOF method(ex. Ashgrizon and Poo, 1991), these velocities are obtained by the continuity equation. In the calculation of solitary

wave, Chan and Street(1970) used vertical extrapolation to obtain these velocities, therefore, the continuity equation is not forced at the surface cells. Actually, the approximation of the former method is acceptable provide the flow in nonperiodic. But it brings considerably errors for periodic problem. Figure 3 shows the calculated results by the original VOF method at different vertical positions.

It is seen that the influence of the free surface boundary increases considerably as the vertical position approaches to the surface. And this effect is more pronounced for the horizontal velocities than the vertical velocities. Accordingly, in our calculation, we used the extrapolation to obtain the horizontal velocities. For example, $u(i + \frac{1}{2}, j)$ in Fig. 2 can be approximated as:

$$u_{i+\frac{1}{2},j} = [u_{i-\frac{1}{2},j}*0.5*(\Delta z_j+\Delta z_{j-1})+u_{i+\frac{1}{2},j-1}*\Delta x_i]/[\Delta x_i+0.5*(\Delta z_j+\Delta z_{j-1})] \quad (15)$$

In case the vertical velocity is also exposed to the air (Fig. 2(b)), the vertical velocity can be obtained by the continuity equation. As for the case shown in Fig. 2(a), there is no way to satisfy the continuity equation in the surface cells. The results of the modified calculation are shown in Fig. 4.

In the numerical simulation, still water level is given at time $t = 0$. No initial superimposed condition has been introduced to the sub-grid scale variables.
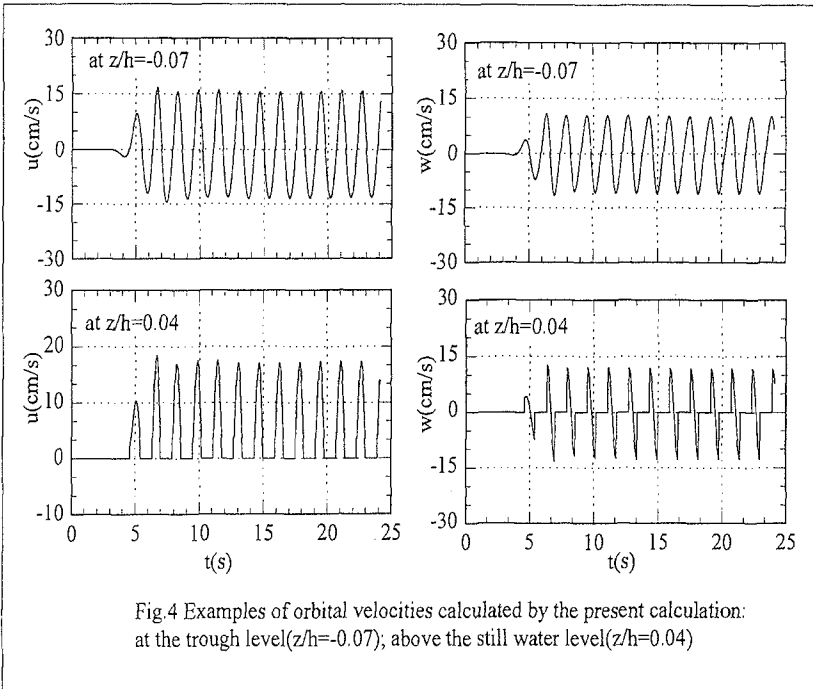

Fig.4 Examples of orbital velocities calculated by the present calculation: at the trough level(z/h=-0.07); above the still water level(z/h=0.04)

Verification with Experimental Measurements

1.Experimental Setup

Finally, breaking waves propagating on a submerged reef are numerically calculated and verified with previous experimental data(Nakamura 1995).

Figure 5 shows the experimental setup and coordinates layout. The wave channel is 17.0 meters long. The model reef is fully impervious and 32.5cm high with a seaward reef face of 1 : 2. Regular waves were generated by a computer controlled piston type wave-maker. Water surface elevations were measured by capacitance-type wave gauges. In the experiment, only six wave gauges were available. The first two gauges(from the wave paddle) were served as reference gauges for incident waves. The other 15 locations of water surfaces were obtained by moving the remained four wave gauges prior to each run. In each run, data were recorded simultaneously from 6 channels at sampling time interval of 50ms. Velocities and pressures were measured at three locations(I, II and III) on the slope of the reef for case A. The $L_1/4$ in the figure denotes a quarter of incident wavelength calculated by linear wave theory. The incident wave characters are given in Table 1 in which x_b is the measured position nearest to the breaking point.

Fig.5 Experimental set-up and coordinates layout
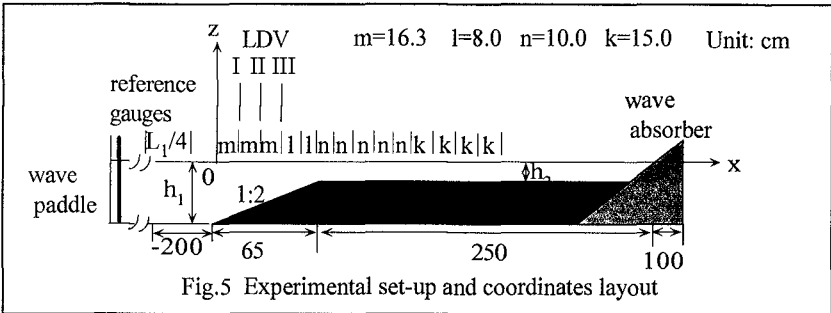
Case	h_1	h_2	T	H_{in}	L_1	x_b
A	45.0cm	12.5cm	1.6s	$6.60cm$	$296.2cm$	$105.0cm$
B	37.5cm	5.0cm	1.6s	$5.64cm$	$276.4cm$	$57.0cm$

Table 1. Simulated cases

In the calculation, incident waves are generated at the left boundary. In order to avoid the pressure divergence at the initial stage, incident wave heights were slowly increased to H_{in}, where H_{in} is the incident wave height obtained by comparing the surface elevations at reference gauge with the physical experiments. The calculated surface elevations were obtained by integration of the F function from the bottom of the channel to the water surface. In the position where air entrainment appears inside the fluid domain, the F function was set to 1 to keep consistency in the experimental measurements. In order to limit effects of wave reflection from the end of the wave channel, the analysis of the experimental data was restricted to the first fully grown-up four or five waves in a record.

2.Calculation Results

Figure 6 shows the normalized vertical distribution of velocities, phase difference and dynamic pressures of case A in which H is the local wave height. To be succinct, only the results of position III are presented here. Besides the experimental results and the numerical simulation, the first order Biesel theory with slight modification(Zhao *et al.*, 1996) is also presented. The general agreements among the analytical solution, the numerical simulation and the experimental results are good. The numerical simulation and the experimental measurement show the same trend of skewness in the vertical velocity and phase difference.

Fig.6 Vertical distribution of maximum and minum orbital velocities, phase differences and dynamic pressures

◆ Measured − − − − − Biesel theory ─o─ Present calculation
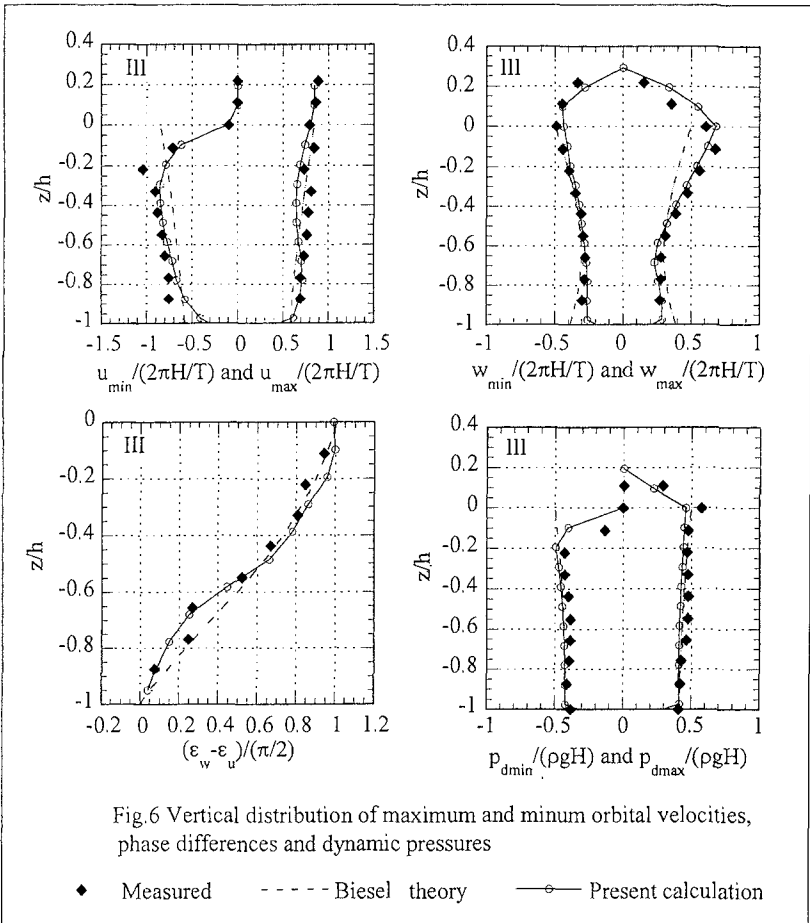
Figure 7 shows the simulated time series of surface elevations together with experimental measurements. Both the measured and calculated surface elevations include the reflective waves from the submerged reef.
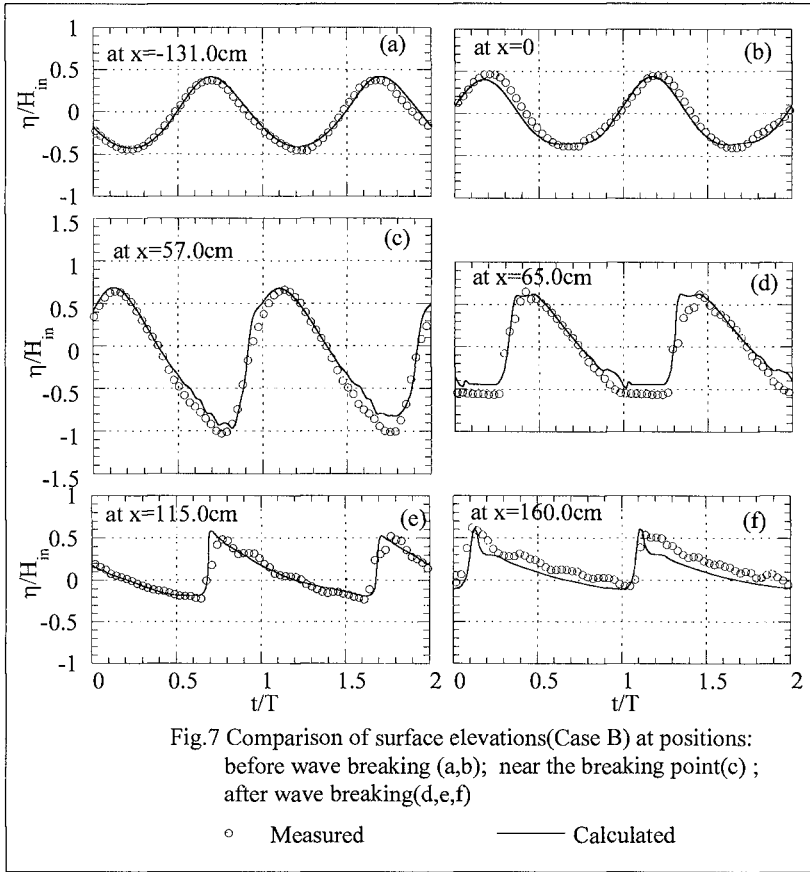
Fig.7 Comparison of surface elevations(Case B) at positions:
before wave breaking (a,b); near the breaking point(c) ;
after wave breaking(d,e,f)
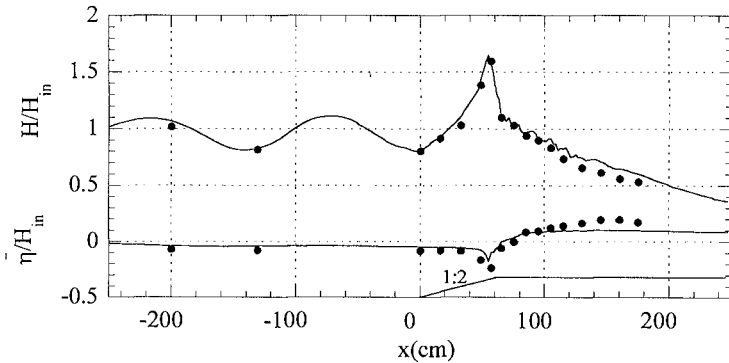
○   Measured   —— Calculated

Fig.8 Comparison of wave height and mean water level distribution

The wave height distribution and mean water level changes are presented in Fig. 8. It is seen that the numerical simulation can give very good results of breaking waves incident on a submerged reef at the reflection side, near the breaking point, and at the transmission region. However, the calculation intends to underestimate the mean water level changes.

Figure 9 shows the filtered vorticity distribution of case B where BP denotes the position of measured breaking point. According to the calculation, the vortices in the figures are generated by two mechanisms, one is by the breaker, and the other one is by the presence of the submerged reef.
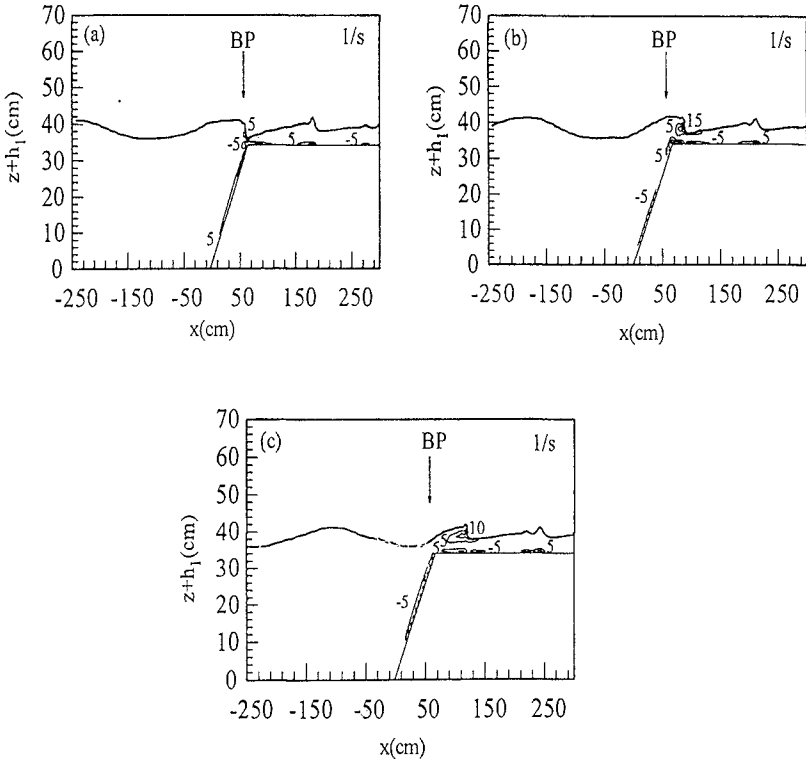

Fig. 9 Vorticity distribution at different phases:
approaching the breaking point(a); after wave breaking(b,c)

The figure indicates that the vortex generated by the breaker is initiated at the toe of the wave front. This vortex is further convected and diffused to almost the whole wave crest.

The other kind of vortices is due to the appearance of the submerged reef. Clockwise and counter-clockwise vortices are generated alternatively depending on the phase of the wave motion. These vortices are not as strong as the one generated by the breaker. They are also convected by the wave.

The figure also shows that for the present condition, the vortex generated by the breaker is confined above the trough level.

It should be noticed that the present model, as well as other two-dimensional models, lacks the three-dimensional vortex stretching mechanism. However, two-dimensional vortex stretching is enabled due to the numerical viscosity.

In Fig.10 we show the spatial distribution of the sub-grid scale eddy viscosity normalized by kinematic viscosity. The calculation shows that the highest eddy viscosity, about 120 times of the kinmeatic viscosity, is appeared slightly after the measured breaking point. The SGS eddy viscosity is smaller than those calculated from Reynolds-averaged equations. This is because that in the present method, only parts of the turbulence whose length scales are smaller than the mesh sizes are modeled. In the RANS models, all fluctuations are modeled. However, it seems premature to say at this stage that the fluctuations appeared in our calculation are turbulence. The fact that F is a step function and the air bubbles which occasionally appeared in the fluid may also contribute to these fluctuations. Further study is necessary. At the present stage, our model can only capture the major flow.
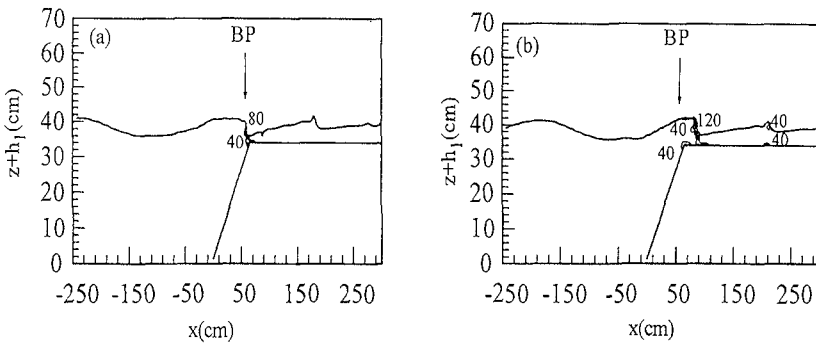

Fig.10 Normalized SGS eddy viscosity at:
approaching the breaking point(a); after wave breaking(b)

Conclusions and Further Improvements

In this paper, the VOF method is applied to simulate breaking waves incident on a submerged reef. In the calculation, an absorbing wave-maker is adopted to handle the wave reflection from the structure. In order to account for the sub-grid scale turbulence, a space filter is applied. The closure is given by Smagorinsky's model. The comparison between the simulation and experimental measurements showed satisfactory agreements. Future work would use a modified SGS model instead of Smagorinsky's SGS model, or develop 3D models to scrutinize the turbulent flow more carefully. The studies of air-water mixing and non-negligible density variations are also necessary.

References

Arai, M., Paul, U.K.,Cheng, L.Y. and Inoue,Y.(1993): A technique for open boundary treatment in numerical wave tanks. *Journal of the Society of Naval Architects of Japan,* **173**, 45-50.

Ashgriz, N. and Poo, J.Y.(1991): FLAIR: Flux line-segment model for advection and interface reconstruction. *J.Comput. Phys.,* **93**, 449-468.

Chan, R.C. and Street, R.L.(1970): A computer study of finite amplitude water waves. *J.Comput. Phys.,* **6** , 68-94.

Deardorff, J.W. (1970): A numerical study of three- dimensional turbulent channel flow at large Reynolds numbers. *J.Fluid Mech.,* **41, part 2** , 453-480.

Hirt, C.W. and Nichols, B. D.(1981): Volume of fluid (VOF) method for the dynamics of free boundaries. *J.Comput. Phys.,* **39** , 201-225.

Hughes, S.A.(1993): Physical models and laboratory techniques in coastal engineering. World Scientific. 333-379.

Kawasaki, K. and Iwata, K.(19978): Numerical analysis of two-dimensional plane wave deformation due to submerged structure(in Japanese). *Proc.of Coastal Engineering, JSCE* , **44(1)** , 81-85

Lemos, C.M.(1992): A simple numerical technique for turbulent flows with free surfaces. *Int. J. Numer. Methods. Fluids.* **15** , 127-146.

Lin, Pengzhi and Liu, Philip L.-F.(1998): A numerical study of breaking waves in the surf zone. *J. Fluid Mech.* **359** , 239-264.

Nakamura, S.(1995): Experimental study on wave velocities on a steep slope bottom(in Japanese). Bachelor thesis. Saitama University.

Petit, H.A.H., van Gent, M.R.A. and van den Bosch, P.(1994) : Numerical simulation and validation of plunging breakers using a 2D Navier-Stokes model. *Proc. 24th Int. Conf. on Coastal Eng., ASCE* , 511-524.

Sabeur, Z.A., Allsop, N.W., Beale, R.G. and Dennis, J.M.(1996): Wave dynamics at coastal structures: development of a numerical model for free surface flow.

Proc. 25th Int. Conf. on Coastal Eng., ASCE, 339-402.

van der Meer, J. W., Petit, H.A.H., van den Bosch, P., Klopman, G. and Broekens, R.D. (1992): Numerical simulation of wave motion on and in coastal structures. *Proc. 23rd Int. Conf. on Coastal Eng., ASCE*, 1772-1784.

van Gent, M.R.A., Tonjes, P., Petit, H.A.H., van den Bosch, P.(1994): Wave action on and in permeble structures. *Proc. 24th Int. Conf. on Coastal Eng., ASCE*, 1739-1753.

Zhao, Q., Nakamura, S. and Tanimoto, K.(1996):Distribution of particle velocities due to waves on very steep slope bottom. IAHR-APD, Langkawi, Maylaysia.

Zhao, Q.(1998):Wave kinematics on a submerged reef with a steep seaward face. Ph.D. thesis, Saitama University.